Klein M, Chakraborty N, Ketterl S.

A comparison of strategies for Direct Numerical Simulation of turbulence chemistry interaction in generic planar turbulent premixed flames.

***Flow, Turbulence and Combustion* (2017)**

DOI: https://doi.org/10.1007/s10494-017-9843-9

A Comparison of Strategies for Direct Numerical Simulation of Turbulence Chemistry Interaction in Generic Planar Turbulent Premixed Flames

Markus Klein*[a], Nilanjan Chakraborty** and Sebastian Ketterl*

*Department of Aerospace Engineering, Universität der Bundeswehr München, Neubiberg, 85577, Germany

** School of Mechanical & Systems Engineering, Newcastle University, Newcastle-Upon-Tyne, NE1 7RU, UK

*[a] Corresponding author

Tel.: +49-89-60042122

Fax: +49-89-60042135

E-mail: Markus.Klein@unibw.de

ABSTRACT

Three different methods to introduce turbulence in the computational domain of Direct Numerical Simulations (DNS) of statistically planar turbulent premixed flame configurations have been reviewed and their advantages and disadvantages in terms of run time, natural flame development, control of turbulence parameters and convergence of statistics extracted from the simulations have been discussed in detail. It has been found that there is no method, which is clearly superior to the other two alternative methods. An analysis has been performed to explain why Lundgren's physical space linear forcing results in an integral length scale which is, independent of the Reynolds number, a constant fraction of the domain size. Furthermore, an evolution equation for integral length scale has been derived, and a scaling analysis of its terms has been performed to explain the evolution of integral length scale in the context of Lundgren's physical space linear forcing. Finally, a modification to Lundgren's forcing approach has been suggested which ensures that the integral length scale settles to a predetermined value so that Direct Numerical Simulations of statistically planar turbulent premixed flames with physical space forcing can be conducted for prescribed values of Damköhler and Karlovitz numbers.

Keywords: Turbulent premixed combustion, Statistically planar flame, Turbulent forcing, Turbulent Inflow.

1. INTRODUCTION

Canonical flow configurations, such as planar flames or flame kernels have the advantage that they allow for well-controlled simulations and turbulence statistics, in particular in the context of Direct numerical simulation (DNS). Statistically planar flames, see exemplarily Fig. 1, which are the focus of this work, have a zero mean flame curvature and the statistical analysis is additionally simplified by the fact that flow quantities vary only in flame normal direction. It is worth noting that the present analysis focuses on statistically planar flames, which have no stretch contribution due to mean shear in contrast to Ref. [1]. A considerable amount of fundamental research in the context of DNS has been conducted using such statistically planar flame configurations.

For statistically planar flames, typically the mean flow parameters and reaction progress variable (which can be defined in terms of normalised value of the species mass fraction or species) are initialised from 1D laminar flame calculations. Three different philosophies can be identified to introduce the turbulence in the computational domain. In one approach (e.g. [2-4]) the whole flow field is initialised using typically a pseudo-spectral method [5] in order to generate divergence free velocity fluctuations. The turbulence decays with time and statistics are recorded after a few eddy turnover times allowing the turbulence to adjust to the flow field. Boundary conditions are taken to be partially non-reflecting for the non-periodic boundaries in the mean direction of flame propagation. A second methodology [6-8] is to use a turbulent inflow condition in order to maintain the desired turbulence level in the computational domain. Statistics are extracted after the flame has reached a statistically stationary state. In order to retain the flame within the computational domain the mean inflow velocity needs to be adjusted because the turbulent flame speed increases with the increasing amount of flame wrinkling. A third variant is to use volume forcing within the whole computational domain in order to ensure

a constant turbulence level. One implementation of this method [9,10] uses a long-wavelength forcing. In a recent work [11] a linear volume forcing term, as suggested by Lundgren [12] and further analysed in [13,14], is used to maintain the desired turbulence intensity. It is argued [11,15] that this kind of forcing is more physical and has good stability properties. Within this third category the Lundgren forcing will be investigated in more detail due to its simplicity of implementation and because its application to turbulent flames is relatively recent. All studies discussed so far used periodic boundary conditions in direction perpendicular to mean flame propagation.

All the aforementioned methodologies have specific advantages and disadvantages which are important to understand and will be discussed in detail in section 3 after introducing the mathematical formulation in section 2. A particular emphasis in this work is given on the characterisation of Lundgren's Forcing and a modification to Lundgren's approach, which will be suggested in section 4, in order to overcome one of its main limitations. Conclusions will be drawn in section 5. Henceforth the following abbreviations will be used for the different flow configurations in the remainder of the paper: DT=Decaying turbulence, IO=inflow/outflow configuration, LF=Lundgren's Forcing.

2. MATHEMATICAL FORMULATION

A well-known three-dimensional compressible DNS code SENGA [2,8,16,17] has been used to simulate the statistically planar turbulent premixed flames. A single step chemistry is used for the purpose of computational economy and because the fundamental turbulence-chemistry interaction behaviour investigated in this work is unaffected by detailed chemistry effects. In SENGA high order finite-difference (10^{th} order central difference scheme for internal grid points and the order of differentiation drops gradually to a single-sided 2^{nd} order scheme at non-

periodic boundaries) and Runge-Kutta (3rd order low-storage) schemes are used for spatial differentiation and explicit time advancement respectively.

The boundary conditions in the mean flame propagation direction are taken to be partially non-reflecting for configurations DT and LF, whereas a subsonic inflow is prescribed for case IO. Boundaries in transverse directions are taken to be periodic in all cases. Initial or inflow data has been generated using a modified version of the method suggested in [18] where the Gaussian filter in axial direction has been replaced by an autoregressive AR1 process in order to avoid excessive filter length in this direction caused by the small time step in the compressible flow solver.

The initial values of the ratio of the root-mean-square turbulent velocity fluctuation and unstrained laminar burning velocity u'/S_L and the integral length scale to thermal flame thickness ratio l/δ_{th} are mentioned separately for each case. The simulation domain is taken to be a rectangular box of $40\delta_{th}$×$20\delta_{th}$×$20\delta_{th}$ which is discretised using a uniform Cartesian grid of 400×200×200 points, ensuring 10 grid points are kept within the thermal flame thickness δ_{th}. For long time runs in the IO configuration the domain length has been extended to $80\delta_{th}$. The heat release parameter $\tau = (T_{ad} - T_0)/T_0$ has been set to 4.5 where T_0 and T_{ad} are the unburned gas temperature and adiabatic flame temperature respectively. Standard values of Prandtl number $Pr = 0.7$, Zel'dovich number $\beta_Z = T_{ac}(T_{ad} - T_0)/T_{ad}^2 = 6.0$ (where T_{ac} is the activation temperature) and ratio of specific heats $\gamma_g = 1.4$ were considered for the present analysis.

3. DISCUSSION

It is obvious that in the decaying turbulence approach the energy spectrum can be prescribed at start of simulation but cannot be predicted in advance at the time when statistics are extracted. The same holds true for the turbulent length scales. The run time is relatively short, typically at the order of 2-4 eddy turnover times $t_e = l/u'$. Typically the value of u'/S_L in the unburned gas ahead of the flame decays by about 50% of its initial value, whereas the value of l/δ_{th} in the fresh gas increases by about 1.7 times by the time statistics were extracted in the DT configuration, indicating that $\mathrm{Re_t}$ decreased by roughly 15% [19]. The data is typically taken from a single frame where turbulent kinetic energy and the global burning rate were not changing rapidly with time as shown in [19]. Moreover, it was demonstrated there that the results remain qualitatively similar halfway through the simulation and that a satisfactory level of convergence has been achieved [19]. It is worth mentioning that it is possible to perform ensemble averaging running the simulation with different initial conditions, if more samples would be required (see e.g. Ref. [20]), for example in the case of higher order statistical moments. The flame evolves in a natural way but there is a history effect in the sense that at the time instant, when the statistics are taken, the flame wrinkling can be exaggerated in comparison to the turbulence intensity prevailing at that point of time. Therefore, results from DT are mostly of qualitative nature and need to be interpreted with due care.

The DT methodology has been criticised because of its unsteady turbulence properties. One way to inject turbulence into the computational domain in order to achieve a statistically steady state is to use a turbulent inflow condition. However, the temporal decay of energy in the DT method has now been replaced by a spatial decay of turbulence, which can be seen from Fig. 2, where an isothermal flow simulation is presented. It should be noted that in Fig. 2 and in the rest of the paper the same reference values are used for quantification of turbulence parameters

in reacting and isothermal flow scenarios, even though S_L and δ_{th} are not relevant to the latter case. The following scaling holds: if, in a decaying frame of reference, turbulence has decayed by about 50% after $3t_e$ one can estimate the spatial distance where the flow has lost 50% of its energy as $x_{50\%} \sim 3t_e S_L$ because in a steady flame the inflow velocity is balanced by the turbulent flame speed which is often of the order of S_L during early stages of flame evolution. A typical value for the integral scale is $l = L/5$ where L is the domain length in transverse direction and let us consider $u'/S_L \approx 5$. Under this assumptions $x_{50\%}$ can be estimated as $x_{50\%} \approx 3L/25$. In other words, instead of a temporal decay of turbulence one has now to deal with an undesirable, relatively fast spatial decay of turbulence. This gives rise to new complications:

1.) The spatial decay of turbulence comes along with an increase of the length scale. It is, for example reported, in Nishiki *et al.* [7] that the turbulence length scale reaches nearly the same size as the computational domain, which is problematic because of the periodic boundary conditions. The location in space where the flame stabilizes is not known *a-priori* and consequently the turbulence parameters in the IO configuration cannot be controlled in a better manner than in the DT configuration.

2.) Experience shows that planar flames in the IO configuration are rather unsteady. As the flame moves back and forth the turbulence parameters change and consequently there is a history effect even in this configuration.

3.) In order to retain the flame inside the computational domain a long extension of the domain in the direction of mean flame propagation is required. If the initial flame location is at the centre of the domain, it is likely that turbulence decays considerably before this point is reached. Under the conditions of low turbulence intensity and large integral length scale, it is possible to obtain an instability due to either combined Landau-Darrieus / thermo-diffusive actions

[21,22] or Rayleigh-Taylor mechanism, introduced by a variable inflow rate in order to account for the changing turbulent flame speed, as mentioned in Aspden *et al.* [9].

Figure 1b shows an illustration of the elongated structures, which eventually can be found in the flame front. This acceleration and deceleration in turn has an impact on the growth rates of the Landau-Darrieus instability as shown in Denet and Haldenwang [23]. For illustration Fig. 3 shows the changing turbulent flame speed for an IO configuration with an inlet velocity disturbance of $u'/S_L = 3$. The turbulent flame speed S_t, evaluated by volume integration of the reaction rate $\dot{\omega}$ of reaction progress variable (i.e. $S_t = (\rho_0 A_P)^{-1} \int_V \dot{\omega} dV$ where ρ_0 is the unburned gas density and A_p is the projected area in the direction of mean flame propagation), starts from the laminar value and subsequently increases. In order to keep the flame inside the domain the inlet velocity was set to a filtered version of the turbulent flame speed. Because of the fact that the turbulent flame brush is at the order of L (see Fig. 1) the inflow velocity has to follow S_t sufficiently rapid to prevent the flame from leaving the domain. The fact that the turbulence level depends on the axial position complicates things further. As a result of this, it is difficult if not impossible to obtain a long term steady state planar flame simulation in the IO case, unless the turbulence intensity is very low of the order of $u'/S_L = 1 - 3$. It is possible to stop the simulation as soon as the flame approaches the inflow boundary but this implies that this configuration loses part of its usefulness because the apparent attraction of this configuration is its potential to generate a statistically steady flame.

It is also worth mentioning that the IO configuration requires considerably longer simulation times until a statistically steady flame brush is obtained. Assuming a computational domain of length $2L$ and that the turbulence should be convected through the flow field at least once, the required simulation time can be estimated, using the same assumptions as before, as $T \sim$

$2L/S_L = 10l/S_L = 10u'/S_L t_e = 50t_e$ for $u'/S_L = 5$. In reality, the turbulent flame speed S_t will be greater than S_L, but this has to be compensated by an even longer computational domain. Furthermore, one flow through time is normally not sufficient and hence the above estimate can be considered as a representative minimum value. Together with the fact that a longer computational domain is required the computational resources are considerably more demanding for the IO configuration compared to the DT case. It is also worth mentioning that this run-time estimate does not include the simulation time for collecting samples.

A positive feature of the (Lundgren) forcing, in contrast to the IO approach, is that the global turbulent kinetic energy (TKE) k can be maintained spatially and temporally at the desired level. On the downside it has been demonstrated in Rosales and Meneveau [13] that the length scale converges to an average scale near 19% (35%) of the domain size based on the estimate $l = u_{rms}^3/\varepsilon$ $(l = k^{\frac{3}{2}}/\varepsilon)$, independent of the initial conditions. This has to do with the fact that in a bounded domain the largest possible wavelengths are limited by the domain size. The Kármán-Howarth-Monin equation [15] shows that, if there exists a steady state forced turbulent flow field, for each individual wavenumber there has to be a balance between the viscous action, the forcing term and the energy flux term, which distributes energy up and down the energy cascade. Therefore, it can be expected that the integral scale will be to some extent smaller than the domain size. This fact can further be demonstrated by assuming a Kolmogorov spectrum of the form $E(\kappa) = C_k \varepsilon^{2/3} \cdot \kappa^{-5/3}$. Then the turbulent kinetic energy can be expressed as:

$$k = \int_{2\pi/\mathrm{L}}^{\pi/\Delta} E(\kappa)\, d\kappa \approx C_k \varepsilon^{2/3} \frac{3}{2} \left(\frac{2\pi}{L}\right)^{-\frac{2}{3}} \tag{1}$$

where $2\pi/L$ and π/Δ are the smallest and largest (note the Nyquist-Shannon Theorem) wavenumbers that can be represented in a domain of dimension L with grid spacing Δ. Hence,

$$\frac{k^{\frac{3}{2}}}{\varepsilon} \approx \frac{\left(C_k \frac{3}{2}\right)^{3/2}}{2\pi} L \tag{2}$$

or in other words $l \sim L$. Using a standard value for the constant $C_k \approx 1.5$ results in $l = 0.54L$ which is a bit larger than the value obtained numerically i.e. $l = 0.35L$ because the Kolmogorov spectrum has no decay at the smallest wavenumbers in contrast to a real spectrum, which accounts for rapid decay of TKE for small wavenumbers. For flame-turbulence interaction this inflexibility in terms of final value of integral length scale l has to be considered as a considerable drawback, because control of the turbulent length scale is often necessary to obtain desired values of Damköhler and Karlovitz numbers in premixed combustion DNS.

An evolution equation for l can be derived by taking the natural logarithm of $l = k^{\frac{3}{2}}/\varepsilon$ which gives $\ln(l) = 3/2\ln(k) - \ln(\varepsilon)$ and finally by differentiation:

$$\frac{1}{l}\frac{Dl}{Dt} = \frac{3}{2}\frac{1}{k}\frac{Dk}{Dt} - \frac{1}{\varepsilon}\frac{D\varepsilon}{Dt} \tag{3}$$

It is worth noting that in this paper $D(\ldots)/Dt$ refers to the total derivative based on global mean velocity (i.e. $D(\ldots)/Dt = \partial(\ldots)/\partial t + \langle u_k \rangle \partial(\ldots)/\partial x_k$, where $\langle \ldots \rangle$ is used to indicate ensemble averaging over the whole domain). For the following analysis an incompressible flow is assumed for the purpose of simplicity. In the context of Lundgren forcing the momentum conservation equation in the *i*th direction takes the following form:

$$\frac{\partial u_i}{\partial t} + u_k \frac{\partial u_i}{\partial x_k} = -\frac{1}{\rho}\frac{\partial p}{\partial x_i} + \frac{1}{\rho}\frac{\partial \tau_{ik}}{\partial x_k} + Q_f u_i \tag{4}$$

where p is the pressure and τ_{ik} is the component of the viscous stress tensor and the last term on the right hand side of Eq. (4) is responsible for physical space forcing where $Q_f = \varepsilon/2k$ ensures that the decay of kinetic energy evaluated over the whole domain can be arrested. It is worth noting here that ε and k are evaluated over the whole domain and thus $Q_f = \varepsilon/2k$ should

be treated as constant for each grid point within the domain at a given time instant. On taking curl of Eq. (4) one obtains the following vorticity transport equation with linear forcing term:

$$\frac{\partial \omega_i}{\partial t} + u_k \frac{\partial \omega_i}{\partial x_k} = \omega_k \frac{\partial u_i}{\partial x_k} + \nu \frac{\partial^2 \omega_i}{\partial x_k \partial x_k} + \frac{\varepsilon}{2k} \omega_i \tag{5}$$

Making use of Eq. (5) and the identity $\varepsilon = \langle 2\nu\Omega \rangle = \langle \nu \omega_i \omega_i \rangle$, which holds true for homogeneous turbulence [24] the transport equation for dissipation can be written as:

$$\frac{D\varepsilon}{Dt} = -2\nu^2 \langle \frac{\partial \omega_k}{\partial x_l} \frac{\partial \omega_k}{\partial x_l} \rangle + \frac{\varepsilon^2}{k} + \langle 2\nu \omega_k \omega_l \frac{\partial u_k}{\partial x_l} \rangle + \nu \frac{\partial^2 \varepsilon}{\partial x_k \partial x_k} - 2\nu \frac{\partial}{\partial x_k} \langle u_k' \Omega' \rangle \tag{6}$$

The first term on the right hand side of Eq. (6) is the turbulent dissipation term denoted T_D the second term is due to the linear forcing T_F and the third term is the turbulent production term T_P. The last two terms vanish in homogeneous turbulence and are not considered further.

The turbulent kinetic energy reaches its steady state relatively fast in the LF approach whereas it takes considerably longer until ε, and l reach their asymptotic limits. During this intermediate state of transition Eq. (3) can be simplified because $Dk/Dt = 0$ and one obtains:

$$\frac{Dl}{Dt} = \frac{l}{\varepsilon} \left(2\nu^2 \langle \frac{\partial \omega_k}{\partial x_l} \frac{\partial \omega_k}{\partial x_l} \rangle - \frac{\varepsilon^2}{k} - \langle 2\nu \omega_k \omega_l \frac{\partial u_k}{\partial x_l} \rangle \right) = \frac{l}{\varepsilon} (T_D + T_F + T_P) \tag{7}$$

For a steady state solution one requires $T_D + T_F + T_P = 0$. In the modelled ε transport equation it is usually assumed $T_P = 0,\ T_D = C_{\varepsilon 2}\, \varepsilon^2/k$. This results in $C_{\varepsilon 2} T_F = T_F$ which is incompatible with the standard value $C_{\varepsilon 2} = 1.92$. Furthermore, it turns out that the turbulent production term is considerably larger that the turbulent forcing term and hence it should not be neglected. Based on the scaling arguments of Tennekes and Lumley [24] one obtains:

$$T_P \sim \varepsilon \frac{k^{\frac{1}{2}}}{\lambda}, \quad \frac{l}{\lambda} \sim \sqrt{\frac{k^{\frac{1}{2}} l}{\nu}} = \sqrt{Re_l} \quad \Rightarrow \quad \frac{l}{\varepsilon} T_p = C_P k^{1/2} \sqrt{Re_l} \tag{8}$$

Fig. 4 shows for three different simulations with turbulent Reynolds numbers $Re_l = 75{,}150{,}300$ that the scalings in Eq. (8) indeed hold true. The definition of the Reynolds number $Re_l = k^{\frac{1}{2}} l/\nu$ and lengths scale $l = k^{\frac{3}{2}}/\epsilon$ (see Eq.(8)) have been chosen to be consistent with

the formalism and methodology of the Lundgren linear forcing. For completeness the corresponding Taylor-scale Reynolds numbers are given by $Re_\lambda = 20.58,\ 28.39,\ 39.88$.

It is also worth reporting the corresponding integral length scales L_{ii} (see Table 1). According to chapter 6 of Pope's book [26] the ratio of L_{11}/L (where L_{11} is the integral scale and $L = k^{3/2}/\varepsilon$) is a function of the Reynolds number and takes for large Reynolds number an asymptotic value of 0.43. Despite the fact that the numbers in Table 1 are taken from one snapshot and are subject to statistical variation they agree reasonably well with the expectation discussed in [26].

Table 1: Different length scales and their interrelationship for the three different Reynolds numbers.

$\boldsymbol{Re_l}$	$\boldsymbol{k^{3/2}/\varepsilon}$	$\boldsymbol{L_{ii}/3}$	$\boldsymbol{(L_{ii}/3)/(k^{3/2}/\varepsilon)}$
75	**0.69**	**0.41**	**0.59**
150	**0.66**	**0.33**	**0.50**
300	**0.64**	**0.28**	**0.44**

In all simulations the computational grid has been adjusted to resolve the Kolmogorov scale. Note that $C_P = 0.29$ has been used. Using $T_D = C_{\varepsilon 2}\,\varepsilon^2/k$ and writing $T_D + T_F + T_P = 0$ as $(-C_{\varepsilon 2} + 1)T_F + T_P = 0$, the expression for T_P Eq. (8) shows that $const \neq C_{\varepsilon,2}(Re_l)$. Hence, we use in the following the symbol C_D instead of $C_{\varepsilon 2}$. It is worth remarking that if T_D and T_P would be combined in one expression one would get $1.0 \times (T_D + T_P) = \varepsilon^2/k$. However, since both terms have the same order of magnitude but entirely different physical nature, it is questionable if these modelling assumptions are reasonable. Using Eq. (8) for a fixed Reynolds number in Eq. (7) gives:

$$\frac{Dl}{Dt} = k^{\frac{1}{2}}\left((C_D - 1) - C_P Re_l^{1/2}\right) = k^{\frac{1}{2}}(C_D - 1) - \left(C_P k^{\frac{3}{4}}\right)/\nu^{\frac{1}{2}} \times \sqrt{l} \quad (9)$$

This is an ordinary differential equation of the form $l' = a - bl^{1/2}$ with real parameters a, b. Knowing that a steady state solution with $l = 0.35L$ will be obtained, a, b can be determined and the ordinary differential equation for l can be solved. Since it has been assumed $Dk/Dt = 0$ the initial value problem has to start from the point in time where k is nearly constant, in this case roughly 0.5 eddy turnover times. The analytical solution for Eq. (9) can be expressed using Lambert's W function [25]. The evolution of l/L against non-dimensional time t/t_e is shown in Fig. 5. In spite of all modelling assumptions the analytical solution predicts the evolution of l (a numerical solution to the Navier-Stokes equation) remarkably well.

Beside the fixed value of l/L there is another disadvantage of the Lundgren forcing which has so far not been reported in the literature. Flame-turbulence interaction for planar flame configurations is normally considered in computational domains with aspect ratio larger than unity, values up to 11 are reported in Savard and Blanquart [11]. However, the forcing method has so far been tested and analysed for cubic domains. In fact, it turns out that the low wavenumbers in direction of the long side of the computational domain interact with the shorter wavelength in transverse direction, which ultimately can lead to the fact that the simulation does not any more converge to the same steady state as reported before and that $k^{\frac{3}{2}}/\varepsilon$ attains considerably larger values. This behaviour is illustrated in Fig. 6 for an isothermal flow situation in two boxes of dimension L^3 and $2L \times L^2$ respectively.

Before suggesting a possible solution to this problem, the flame-turbulence interaction in the LF approach will be discussed further. Turbulence decays across the flame and length scales increase due to dilatation and a rise in viscosity with heat release, whereas the forcing tries to

enforce a constant level of turbulence on both sides of the flame brush. In this sense, the flame-turbulence interaction is not physical if the forcing is applied to the whole computational domain, and it is likely that an unrealistically high level of turbulence is obtained on the burned gas side combined with too small turbulent scales if the forcing is applied both on unburned and burned gas sides of the flame. It is worth mentioning that such an approach requires a modification of the procedure reported in Lundgren [12] in two aspects:

1.) If a compressible variable density solver is used, the equations look slightly different and have to be modified according to the suggestion of Rosales and Meneveau [13] where $Q_f = \left[\varepsilon + \langle u_j \, \partial p/\partial x_j \rangle\right]/2k$. However, it has been found by the authors that for low Mach number flows the incompressible formulation gives results nearly identical to the compressible version.

2.) Instead of determining the forcing parameters globally, an averaging in homogeneous direction should be considered.

Instead of global forcing, the forcing alternatively could be applied only to the reactant side. This would allow for a free flame development and the integral length scales could increase across the flame front. However, starting from an already relatively large fraction of the domain size, according to the LF formulation, it is possible that the turbulent scales might reach a critical limit during the course of the simulation, which makes them incompatible with the assumption of periodic boundary conditions.

Table 2 summarizes the most important properties of the three different approaches to introduce turbulence in planar flame configurations.

Table 2: Properties of the three different flow setups

Method	Typical run time	TKE control	Control of length scales	Natural Flame development
Decaying Turbulence	~2-4 EDT [2,3]	At $t = 0$, but TKE decays with time	At $t = 0$, but length scales increase with time	Yes, but with history effect
Inlet / Outlet	~3-5 EDT [7] ~2-17 EDT [27]	At $x = 0$, but TKE decays in space	At $x = 0$, but length scales increase in space	Possibility of L-D & R-T Instability
Lundgren's Forcing	~20 EDT [13] ~20 EDT [11]	Yes	No	No, if forcing is applied to burned side

The forcing term $\vec{f}$ in the physical space forcing used in the LF method for incompressible flows is given by:

$$\vec{f} = (\varepsilon/2k)\,\vec{u} \tag{10}$$

It should be noted that using a spatially varying constant of proportionality, instead of the global value $\varepsilon/2k$ in Eq. (10), implies that the forcing term is not any more guaranteed to be divergence free. This would be the case in forcing variants where homogeneous averaging is used and as well for unburned gas forcing. Moreover, it is not clear how the flame turbulence interaction modifies the length scales, which are known from isothermal forcing. Finally, it needs to be noted that unburned gas forcing results in a too low turbulent kinetic energy if Eq. (10) is used without any modification. It is assumed that the turbulence is damped at the flame front because forcing is applied on one side of the flame front (or domain) but not on the other side. Similar to the IO method, the (Lundgren) forcing method requires a rather long run time before a statistically steady state is achieved.

4. BAND-WIDTH FILTERED FORCING

In order to avoid the problem with uncontrolled growth of length scales in rectangular domains, it is suggested to make the forcing proportional to a high pass filtered velocity fluctuation, in this work which is given by $\bar{u}_i{}^{HP} = u_i - \bar{u}_i$,where $\overline{(\ldots)}$ is a conventional low pass filter

typically used in the context of LES with a 1D Gaussian filter kernel given by $G(x) = \left(6/\pi \mathrm{L}_\mathrm{f}^2\right)^{1/2} \exp(-6\, x^2/L_f^2)$ and where L_f is a filter length scale at the order of L. The filtering is only applied in axial direction, because the low wave number fluctations in this direction have been identified as the root cause for the undesirable behaviour described earlier. The constant of proportionality in Eq. (10), i.e. $\varepsilon/2k$, is based on the assumption that the forcing term is proportional to $\vec{u}$ whereas in the band filtered approach the forcing is proportional to $\bar{\vec{u}}^{HP}$. Instead of modifying Eq. (10) a simple control mechanism is used here, a method similar to the one suggested by Mallouppas *et al.* [35], such that the forcing term takes the following form:

$$\vec{f} = \max[0, (k_{target} - k)/(\Delta t k_{target})]\ \bar{\vec{u}}^{HP} \tag{11}$$

This provided very stable calculations in terms of turbulent kinetic energy. The evolution of $k^{\frac{3}{2}}/\varepsilon$ in combinations with different high-pass filters is shown in Fig. 7. First of all, if L_f is at the order of L, it can be seen that the wavelength remains bounded and at the same order of magnitude (i.e. $0.35L$) even on a rectangular domain. It has been checked that this also holds true for run times considerably longer to those shown if Fig. 7. It is however interesting to note that the same methodology can be used not only to prevent unwanted growth of $k^{\frac{3}{2}}/\varepsilon$ but also to achieve considerably smaller length scales compared to the original approach, see Fig. 7 and the instantaneous velocity fields shown in Fig. 8. It is worth noting that the simulations were run for isothermal conditions in Figs. 7 and 8. Fig. 9 (a) shows one-dimensional energy spectra with Kolmogorov scaling for the filtered forcing method in comparison to unfiltered forcing in a cubic domain. It can be seen that filtered forcing with characteristic filter length $L_f = L$ yields an energy spectrum, which is in close agreement with the unfiltered forcing and especially that the normalized spectra nearly collapse at high wave numbers. Furthermore, the straight line behavior in the log-linear plot of the compensated spectra in Fig. 9 (b) indicates the exponential

decay of the spectra at highest wavenumbers. The extensive characterization of the spectra for the original forcing approach (black line) can be found in reference [12]. From Fig. 9 it is clear that the filtered forcing does not disturb the dissipation range in comparison to the unfiltered Lundgren forcing.

It is worth noting that each forcing method is subject to some approximations. Furthermore, according to the best knowledge of the authors, there is not a single theoretical spectrum that would describe isotropic turbulent flows (apart from the fact that the inertial range scaling seems to be an accepted fact). For many years researchers carried out long wavelength forcing (see [9,10]) because it was believed that it will not affect the small scale statistics. However, as pointed out by Lundgren [12] the spectral width of the forcing has a noticeable effect on inertial range statistics. In fact, this has been one of the motivations in [12] for investigating the linear forcing. For the original version of the Lundgren forcing the shape of the spectrum cannot be prescribed. Instead, the scales adjust themselves to a specific shape. For the filtered forcing as suggested in this work, the shape of the spectrum will depend on the specific filter function. For simplicity, a Gaussian filter has been used for the current analysis, but arbitrary filter functions are possible and would help to adjust the spectrum to a specific shape. The choice of such a filter function is not a trivial problem and such an investigation will be left for future work.

The linear forcing has been extensively studied in Refs. [12-15]. In order to demonstrate that the newly proposed filtered linear forcing is physical and does not produce any peculiar artefacts in turbulence dynamics we analyse the filtered forcing in some more detail where the filter width has been set to $L_f = 0.25L$. The filtered linear forcing has been analysed with respect to the alignment of strain-rate tensor eigenvalues with vorticity as well as intermittency, which is closely related to the non-Gaussian behaviour of velocity and velocity derivative PDFs.

For the first purpose, strain rate has been decomposed into its most extensive, intermediate and most compressive principal strain components (i.e. e_α, e_β and e_γ respectively) and their alignments with the vorticity vector $\vec{\omega}$ has been analysed by looking at the angles $\theta_\alpha, \theta_\beta$ and θ_γ between $\vec{\omega}$ and e_α, e_β and e_γ, respectively. It is worth noting that $\vec{\omega}$ aligns predominantly with e_β in (non-reacting) turbulent flows [28-30] and this is exactly reflected in the probability density functions (PDFs) of $|cos\theta_\alpha|, |cos\theta_\beta|, |cos\theta_\gamma|$ shown in Fig. 10.

According to She *et al*. [33] it has been well verified that the probability distribution of the full velocity field is basically Gaussian but the deviation from a Gaussian distribution becomes significantly more pronounced at small scales. This is clearly reflected in Fig. 11 where PDFs of the velocity fluctuations using the full velocity spectrum (a) as well as high pass filtered velocity fluctuations corresponding to high wave number modes (b) are shown. Furthermore, it is known [33] that the distribution of the velocity derivatives deviates from a Gaussian distribution. Longitudinal as well as transversal velocity derivative PDFs (see Figs. 11 (c) respectively (d)) are characterised by exponential tails. Whereas the lateral derivative skewness is close to zero (see Fig. 11 (d)) due to the symmetry of the Navier-Stokes equations, the asymmetry in the longitudinal velocity derivative is clearly seen in Fig. 11 (c). The behaviour in Fig. 11 is qualitatively consistent with experimental [31,32] and numerical findings reported in literature [33,34].

Finally, the filtered forcing is applied to a statistically planar turbulent premixed flame case, but the forcing is only active on the unburned gas side. This is achieved by multiplying the expression in Eq. (11) by $(1 - c)$, where c is the reaction progress variable. Turbulence intensity has been set to $u'/S_L = 3$ and the filter length scale to $L_f = 0.25L$. Figure 12 shows small turbulent structures interacting with the flame and considerably more small scale flame

wrinkling in comparison to Fig. 1. Nevertheless, more experience will be needed to understand possible drawbacks of forcing only on the reactant side.

Despite the fact that implementation of spectral forcing for codes based on physical space solvers is both difficult and expensive, this forcing method, which dates back to the work of Eswaran and Pope [36], is very flexible in the sense that integral scales can be very effectively controlled (e.g. any fraction of the domain size can be achieved). Furthermore, in this framework the energy injection spectra can be of arbitrary complexity.

5. CONCLUSIONS

Different strategies for DNS of turbulence-chemistry interaction for statistically planar turbulent premixed flames have been investigated in this analysis. Each method has been shown to have considerable shortcomings, compared to the other alternative approaches. It also becomes clear that the conventional and the simplest approach, the decaying turbulence configuration is probably not really worse than the other alternative more complex and expensive methods. Nevertheless, Lundgren's linear forcing seems to be a promising approach for obtaining statistically stationary flames, and an emphasis is given here on the analysis of this approach. Integrating a Kolmogorov spectrum from the largest to the smallest scales on a given computational grid yields a length scale, which is a constant fraction of the domain size. A transport equation for $l = k^{3/2}/\varepsilon$ for forced flows has been derived using the transport equations of turbulent kinetic energy k and its dissipation rate ε. A scaling analysis shows that the turbulent production term has the same order of magnitude as the dissipation term and should not be neglected. Furthermore, the model expressions for the turbulent production and dissipation terms have been found to be Reynolds number dependent. The scaling relations yield a simplified ordinary differential equation for the evolution of $l = k^{3/2}/\varepsilon$. The analytical

solution of the aforementioned ordinary differential equation shows satisfactory agreement with numerical simulations. Finally, a suggestion has been made to overcome some of the observed problems related to the linear forcing. It has been found that the length scale can be adjusted to a desired value by making the forcing term proportional to a high pass filtered value of velocity. A first application of this modified approach to a turbulent premixed planar flame yields promising results.

ACKNOWLEDGEMENTS

The authors are grateful to N8, ARCHER and EPSRC for computational support.

CONFLICT OF INTEREST

The authors declare that they have no conflict of interest.

REFERENCES

1. Trouvé, A., The production of premixed flame surface area in turbulent shear flow, Combustion and Flame, 99, 687-696 (1994).
2. Chakraborty N., Klein M. and Cant R.S., Effects of Turbulent Reynolds Number on the Displacement Speed Statistics in the Thin Reaction Zones Regime of Turbulent Premixed Combustion, Journal of Combustion, vol. 2011, Article ID 473679, (2011).
3. Han I. and Huh K.Y., Roles of displacement speed on evolution of flame surface density for different turbulent intensities and Lewis numbers in turbulent premixed combustion. Combustion and Flame, 152, pp. 194-205, (2008).
4. Kim S.H. and Pitsch H., Scalar gradient and small-scale structure in turbulent premixed combustion. Physics of Fluids, 19, 115114, (2007).
5. Rogallo, R.S., Numerical experiments in homogeneous turbulence, *NASA Technical Memorandum 81315*, NASA Ames Research Center, California (1981).
6. Rutland C.J. and Cant R.S., Turbulent transport in premixed flames, Proc.Summer Program, Center for Turbulence Research, pp. 75-94, (1994).
7. Nishiki S., Hasegawa T. Borghi R. and Himeno R., Modelling of turbulent scalar flux in turbulent premixed flames based on DNS databases. Combustion Theory and Modelling, 10, No. 1, pp. 39-55, (2006).
8. Chakraborty N. and Cant S., Unsteady effects of strain rate and curvature on turbulent premixed flames in an inflow–outflow configuration, Combustion and Flame 137, 129–147, (2004).
9. Aspden A.J., Day M. S. and Bell J.B., Turbulence-flame interactions in lean premixed hydrogen: transition to the distributed burning regime. J. Fluid Mech. 680, pp. 287-320, (2011).

10. Poludnenko A.Y. and Oran E.S., The interaction of high-speed turbulence with flames: Global properties and internal flame structure. Combustion and Flame, 157, pp. 995-1011, (2010).
11. Savard B. and Blanquart G., Broken reaction zone and differential diffusion effects in high Karlovitz n-C7H16 premixed turbulent flames. Combustion and Flame, 162, pp. 2020-2033, (2015).
12. Lundgren T., Linear Forced Isotropic Turbulence in Annual Research Briefs, Center for Turbulence Research, Stanford, pp. 461–473, (2003).
13. Rosales C and Meneveau C., Linear forcing in numerical simulations of isotropic turbulence: Physical space implementations and convergence properties. Physics of Fluids, 17, 095106, (2005).
14. Carroll P.L. and Blanquart G., A proposed modification to Lundgren's physical space velocity forcing method for isotropic turbulence. Physics of Fluids, 25, 105114, (2013).
15. Carroll P.L. and Blanquart G., The effect of velocity field forcing techniques on the Karman–Howarth equation, Journal of Turbulence, 15, 429-448, (2014).
16. Jenkins K.W., Klein M., Chakraborty N. and Cant R.S.2006, Effects of strain rate and curvature on the propagation of a spherical flame kernel in the thin-reaction-zones regime, Combustion and Flame, 145, 415-434, (2006).
17. Chakraborty N., Klein M. and Cant R.S., Stretch rate effects on displacement speed in turbulent premixed flame kernels in the thin reaction zones regime, Proceedings of the Combustion Institute, 31, 1385-1392, (2007).
18. Klein M., Sadiki A. and Janicka J., A Digital Filter Based Generation of Inflow Data for Spatially Developing Direct Numerical or Large Eddy Simulations. J. Comp. Physics, 186, 652-665, (2003).

19. Chakraborty N. and Cant R.S., Effects of Lewis number on flame surface density transport in turbulent premixed combustion, Combustion and Flame, 158, 1768-1787, (2011).
20. Chakraborty N., Wang. L and Klein M., Streamline segment statistics of premixed flames with nonunity Lewis numbers, Physical Review E, 89, 033015 (2014).
21. Matalon M. and Matkowsky B.J., Flames as gasdynamic discontinuities. Journal of Fluid Mechanics, 124, pp. 239-259, (1982).
22. Chaudhuri S., Akkerman V. and Law C.K., Spectral formulation of turbulent flame speed with consideration of hydrodynamic instability, Physical review E, 84, 026322, (2011).
23. Denet B. and Haldenwang P., A Numerical Study of Premixed Flames Darrieus-Landau Instability, Combust. Sci. and Tech. 104, 143-167, (1995).
24. Tennekes H, Lumley JL. A first course in turbulence, 1st Edition, MIT Press, Cambridge, Massachusetts, USA; 1972.
25. Robert M. Corless, G. H. Gonnet, D. E. G. Hare, D. J. Jeffrey, and D. E. Knuth, "On the Lambert W Function", Advances in Computational Mathematics, volume 5, 329-359 (1996).
26. Pope S.B., Turbulent flows, Cambridge University Press, (2000).
27. Wacks, D. H., Chakraborty, N., Klein, M., Arias, P. G. & Im, H. G. Flow topologies in different regimes of premixed turbulent combustion: A direct numerical simulation analysis. Phys. Rev. Fluids 1, 083401 (2016).
28. Ashurst W, Kerstein A, Kerr RM. & Gibson CH. Alignment of vorticity and scalar gradient with strain rate in simulated Navier–Stokes turbulence, Phys. Fluids A, 30, 2343 (1987).
29. Majda AJ. Vorticity, turbulence, and acoustics in fluid flow, SIAM Rev., 33, 349, (1991).
30. Jimenez J. Kinematic alignment effects in turbulent flows, Phys. Fluids A, 4, 652, (1992).

31. Batchelor G., Townsend A., The nature of turbulent motion at large wave-numbers, in: Proceedings of the Royal Society of London A: Mathematical, 240 Physical and Engineering Sciences, volume 199, The Royal Society, pp. 238-255, (1949).
32. Monin A. S., Yaglom A. M., Statistical Fluid mechanics, volume II: Mechanics of turbulence, volume 2, Courier Corporation, (2013).
33. She Z.-S., Jackson E. and Orszag S. A., Scale-dependent intermittency and coherence in turbulence, Journal of scientific computing 3, 407-434, (1988).
34. Yamamoto K. and Kambe T., Gaussian and near-exponential probability distributions of turbulence obtained from a numerical simulation, Fluid Dynamics Research 8, 65-72, (1991).
35. Mallouppas G., George W.K. and van Wachem B.G.M., New forcing scheme to sustain particle-laden homogeneous and isotropic turbulence, Physics of Fluids 25, 083304, (2013).
36. Eswaran V. and Pope S.B., An examination of Forcing in Direct Numerical Simulations of Turbulence, Computers and Fluids 16, 257-278, (1988).

TABLES

Table 1: Different length scales and their interrelationship for the three different Reynolds numbers.

Re_l	$k^{3/2}/\varepsilon$	$L_{ii}/3$	$(L_{ii}/3)/(k^{3/2}/\varepsilon)$
75	**0.69**	**0.41**	**0.59**
150	**0.66**	**0.33**	**0.50**
300	**0.64**	**0.28**	**0.44**

Table 2: Properties of the three different flow setups

Method	**Typical run time**	**TKE control**	**Control of length scales**	**Natural Flame development**
Decaying Turbulence	~2-4 EDT [2,3]	At $t = 0$, but TKE decays with time	At $t = 0$, but length scales increase with time	Yes, but with history effect
Inlet / Outlet	~3-5 EDT [7] ~2-17 EDT [27]	At $x = 0$, but TKE decays in space	At $x = 0$, but length scales increase in space	Possibility of L-D & R-T Instability
Lundgren's Forcing	~20 EDT [13] ~20 EDT [11]	Yes	No	No, if forcing is applied to burned side

FIGURE CAPTIONS

Figure 1. Instantaneous view of c isosurfaces. The value of c increases from 0.1 to 0.9 from yellow to red. (a) DT method. Initial length scale l corresponds to $l/\delta_{th} = 2$ or $l/L = 1/10$ and inlet velocity fluctuation has been set to $u'/S_L = 5$. (b) IO configuration where inflow length scale l corresponds to $l/\delta_{th} = 2$ or $l/L = 1/10$ and inlet velocity fluctuation has been set to $u'/S_L = 3$. (c) LF forcing with target velocity fluctuation of $u'/S_L = 3$.

Figure 2: Decay of turbulent kinetic energy with normalised distance x/l, averaged over the $y-z-$plane, in an isothermal IO configuration. Results are exemplarily shown for an inflow length scale l corresponding to $l/\delta_{th} = 2$ or $l/L = 1/10$ and an inlet velocity fluctuation equivalent to $u'/S_L = 3$.

Figure 3: Variation of turbulent flame speed over time for an IO configuration. Inflow length scale l corresponds to $l/\delta_{th} = 2$ or $l/L = 1/10$ and an inlet velocity fluctuation of $u'/S_L = 3$ is imposed.

Figure 4: Temporal evolution of the production term $\left(T_p \frac{l}{\varepsilon}\right)/C_p k^{\frac{1}{2}} Re_l^{\frac{1}{2}}$ in the l transport equation for three simulations with different turbulent Reynolds number. Due to the linear forcing turbulence intensity is maintained at $u'/S_L = 3$ and the length scale converges to the same asymptotic fraction of the domain size $l/L = 0.35$.

Figure 5: Evolution of l/L over non-dimensional time t/t_e for an isothermal Lundgren forced flow. Analytical solution of model equation is shown in red, Navier-Stokes solution is shown in blue. Due to the linear forcing turbulence intensity is maintained at an equivalent value of $u'/S_L = 3$.

Figure 6: Development of the normalized length scale $(k^{3/2}/\varepsilon)/L$ with non-dimensional time t/t_e in a cubic domain and a rectangular domain, for an isothermal Lundgren-forced flow. Due to the linear forcing turbulence intensity is maintained at an equivalent value of $u'/S_L = 3$.

Figure 7: Development of the normalized length scale $(k^{\frac{3}{2}}/\varepsilon)/L$ with non-dimensional time t/t_e in a rectangular domain for an isothermal Lundgren forced flow, where the forcing term is filtered with a high pass filter of characteristic length L_f. Due to the linear forcing turbulence intensity is maintained at an equivalent value of $u'/S_L = 3$.

Figure 8: Instantaneous velocity field in a rectangular domain with a high pass filtered forcing term of characteristic length $L_f = L$ (top) $L_f = L/4$ (bottom) for an isothermal flow situation. Due to the linear forcing turbulence intensity is maintained at an equivalent value of $u'/S_L = 3$.

Figure 9: One dimensional energy spectra using the filtered forcing method in an isothermal scenario in comparison to the unfiltered forcing in a cubic domain. (a) Spectra with Kolomogorov scaling (b) Compensated energy spectra in a linear-log plot.

Figure 10: Probability density functions (PDFs) of $|cos\theta_\alpha|, |cos\theta_\beta|, |cos\theta_\gamma|$ representing the alignment of vorticity with the most extensive, intermediate and most compressive principal strain rate.

Figure 11: Probability density function characteristics for filtered linear forcing using $L_f = 0.25L$ in a log-linear plot. Displayed are velocity fluctuations using the full velocity spectrum (a), high pass filtered velocity fluctuations corresponding to high wave number modes (b), longitudinal (c) and transversal (d) velocity derivatives using the full velocity spectrum.

Figure 12: Planar flame with filtered forcing applied to the unburned gas side only. Results are exemplarily shown for a (high pass filter) filter size of $L_f/\delta_{th} = 5$ $(L_f/L = 0.25)$ and a target velocity fluctuation of $u'/S_L = 3$.

FIGURES

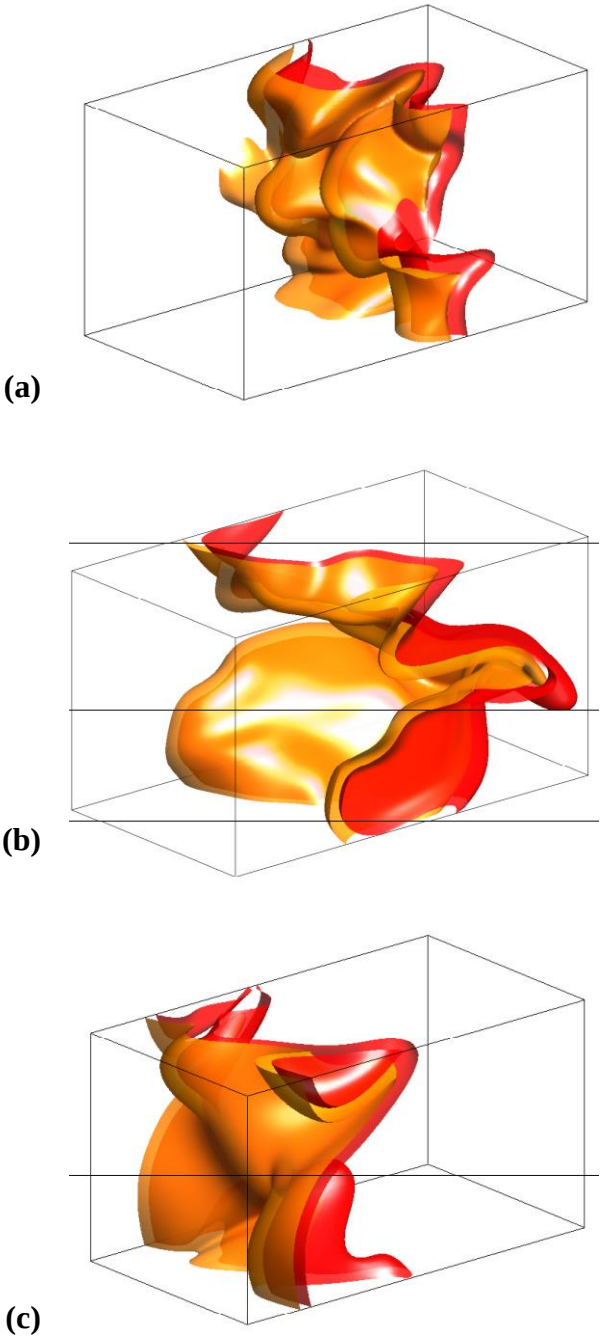

Figure 1. Instantaneous view of c isosurfaces. The value of c increases from 0.1 to 0.9 from yellow to red. (a) DT method. Initial length scale l corresponds to $l/\delta_{th} = 2$ or $l/L = 1/10$ and inlet velocity fluctuation has been set to $u'/S_L = 5$. (b) IO configuration where inflow length scale l corresponds to $l/\delta_{th} = 2$ or $l/L = 1/10$ and inlet velocity fluctuation has been set to $u'/S_L = 3$. (c) LF forcing with target velocity fluctuation of $u'/S_L = 3$.

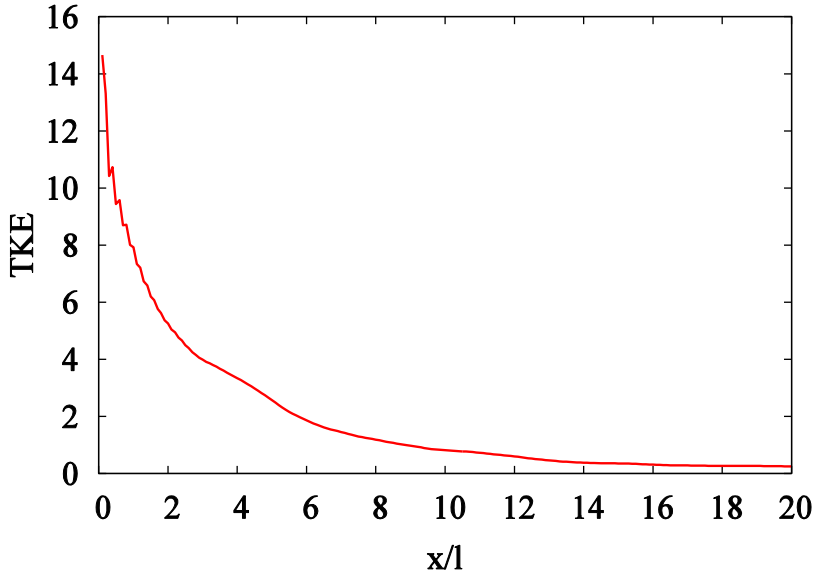

Figure 2: Decay of turbulent kinetic energy with normalised distance x/l, averaged over the $y-z$ −plane, in an isothermal IO configuration. Results are exemplarily shown for an inflow length scale l corresponding to $l/\delta_{th} = 2$ or $l/L = 1/10$ and an inlet velocity fluctuation equivalent to $u'/S_L = 3$.

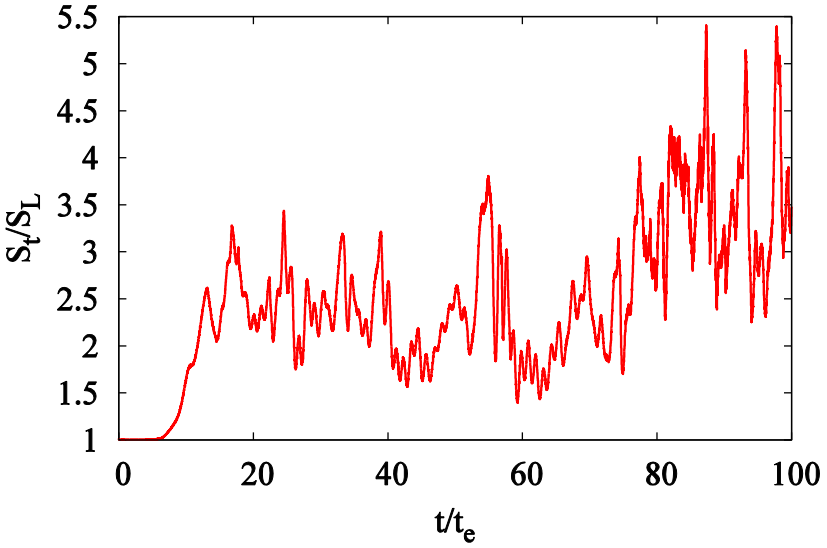

Figure 3: Variation of turbulent flame speed over time for an IO configuration. Inflow length scale l corresponds to $l/\delta_{th} = 2$ or $l/L = 1/10$ and an inlet velocity fluctuation of $u'/S_L = 3$ is imposed.

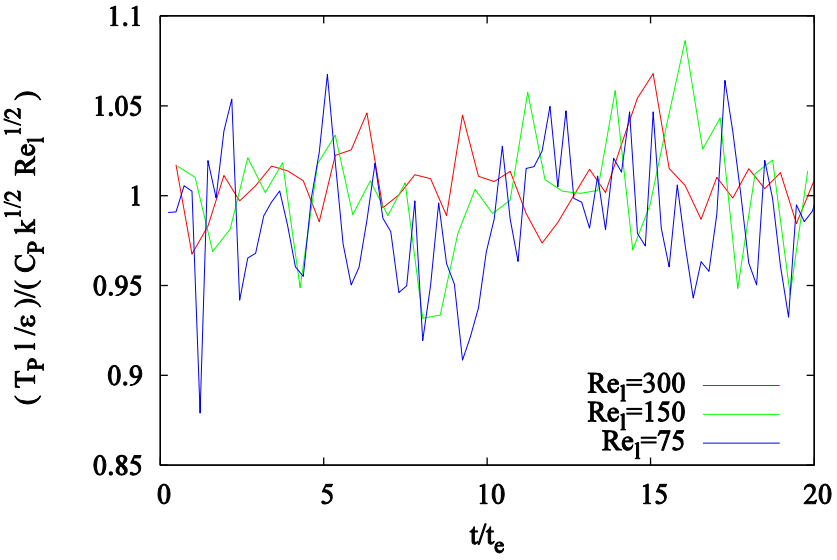

Figure 4: Temporal evolution of the production term $\left(T_p \frac{l}{\varepsilon}\right)/C_p k^{\frac{1}{2}} Re_l^{\frac{1}{2}}$ in the l transport equation for three simulations with different turbulent Reynolds number. Due to the linear forcing turbulence intensity is maintained at $u'/S_L = 3$ and the length scale converges to the same asymptotic fraction of the domain size $l/L = 0.35$.

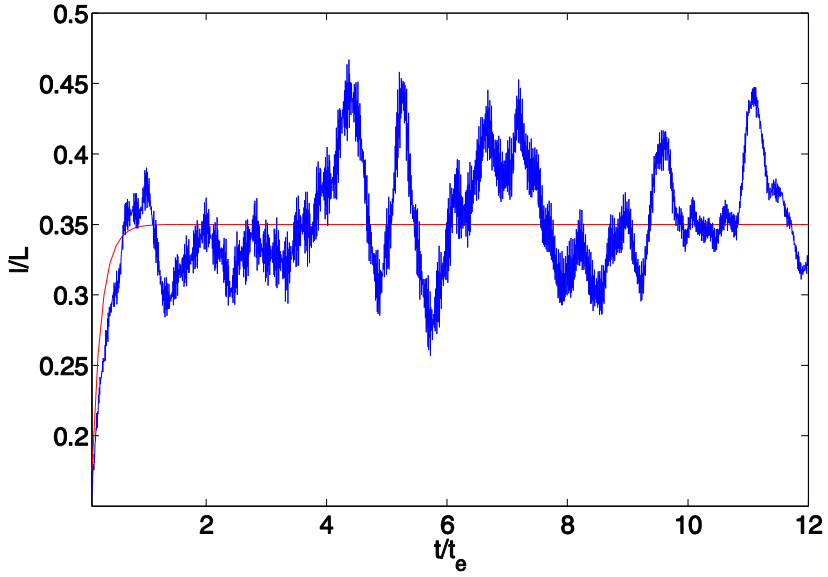

Figure 5: Evolution of l/L over non-dimensional time t/t_e for an isothermal Lundgren forced flow. Analytical solution of model equation is shown in red, Navier-Stokes solution is shown in blue. Due to the linear forcing turbulence intensity is maintained at an equivalent value of $u'/S_L = 3$.

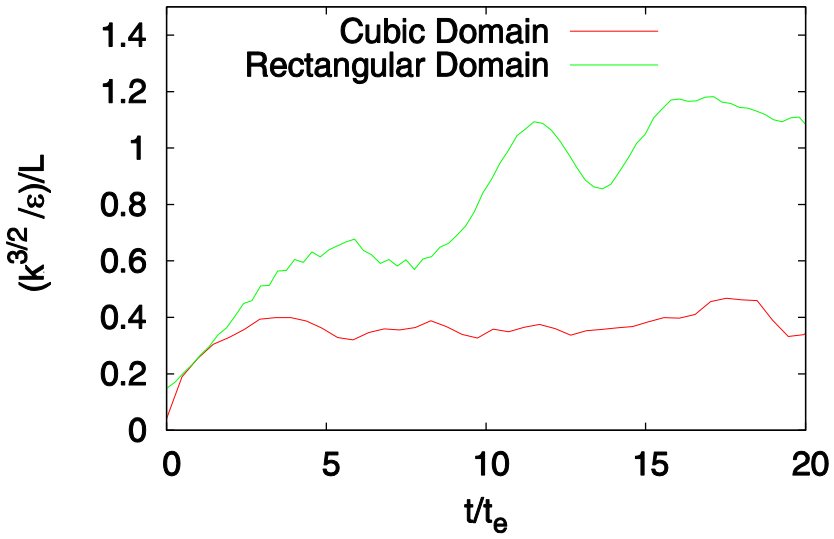

Figure 6: Development of the normalized length scale $(k^{3/2}/\varepsilon)/L$ with non-dimensional time t/t_e in a cubic domain and a rectangular domain, for an isothermal Lundgren-forced flow. Due to the linear forcing turbulence intensity is maintained at an equivalent value of $u'/S_L = 3$.

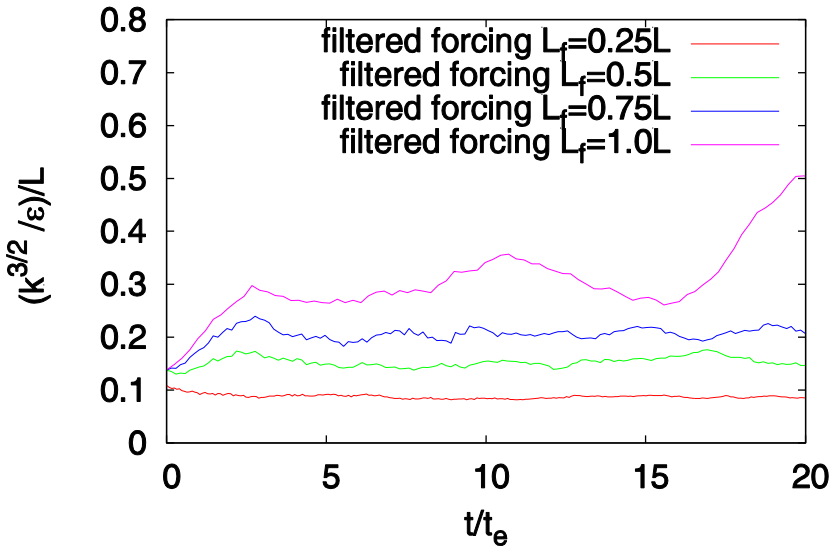

Figure 7: Development of the normalized length scale $(k^{\frac{3}{2}}/\varepsilon)/L$ with non-dimensional time t/t_e in a rectangular domain for an isothermal Lundgren forced flow, where the forcing term is filtered with a high pass filter of characteristic length L_f. Due to the linear forcing turbulence intensity is maintained at an equivalent value of $u'/S_L = 3$.

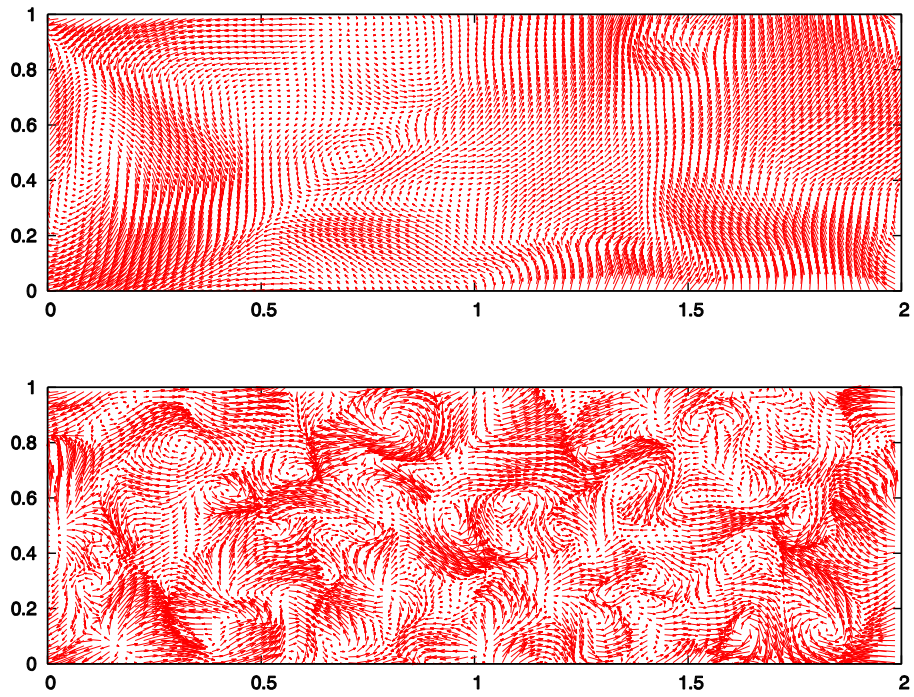

Figure 8: Instantaneous velocity field in a rectangular domain with a high pass filtered forcing term of characteristic length $L_f = L$ (top) $L_f = L/4$ (bottom) for an isothermal flow situation. Due to the linear forcing turbulence intensity is maintained at an equivalent value of $u'/S_L = 3$.

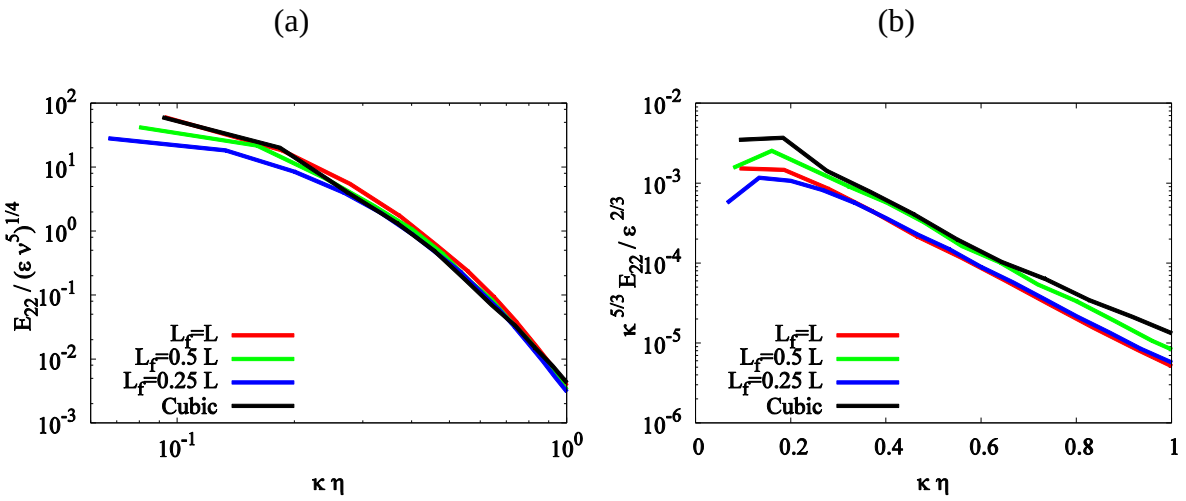

Figure 9: One dimensional energy spectra using the filtered forcing method in an isothermal scenario in comparison to the unfiltered forcing in a cubic domain. (a) Spectra with Kolomogorov scaling (b) Compensated energy spectra in a linear-log plot.

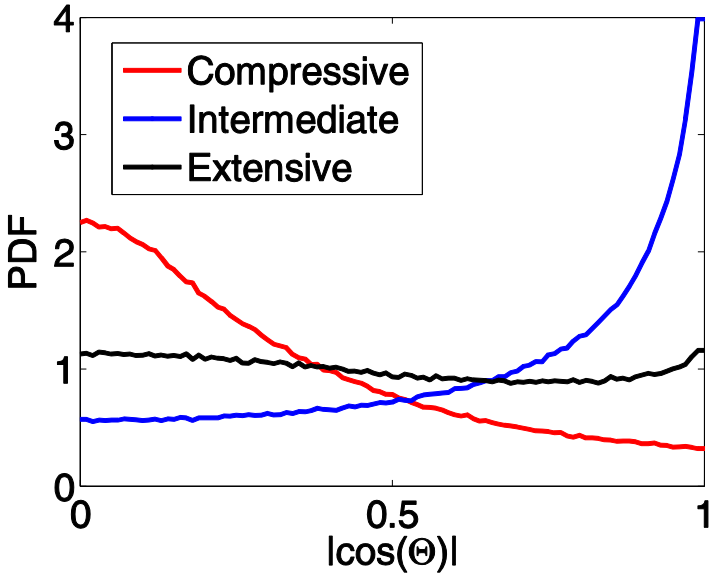

Figure 10: Probability density functions (PDFs) of $|cos\theta_\alpha|, |cos\theta_\beta|, |cos\theta_\gamma|$ representing the alignment of vorticity with the most extensive, intermediate and most compressive principal strain rate.

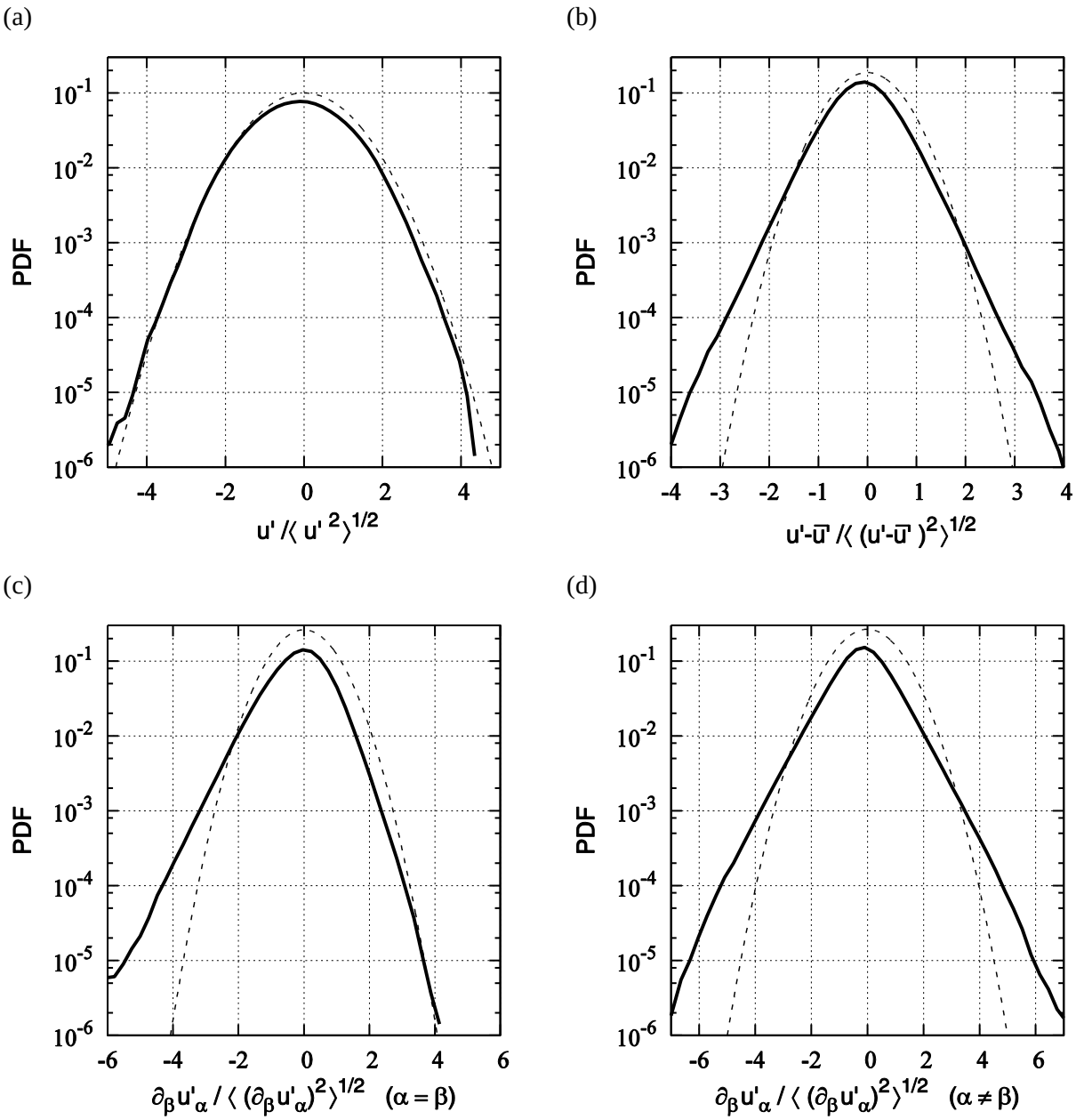

Figure 11: Probability density function characteristics for filtered linear forcing using $L_f = 0.25L$ in a log-linear plot. Displayed are velocity fluctuations using the full velocity spectrum (a), high pass filtered velocity fluctuations corresponding to high wave number modes (b), longitudinal (c) and transversal (d) velocity derivatives using the full velocity spectrum. A Gaussian PDF (dashed line) is shown for reference.

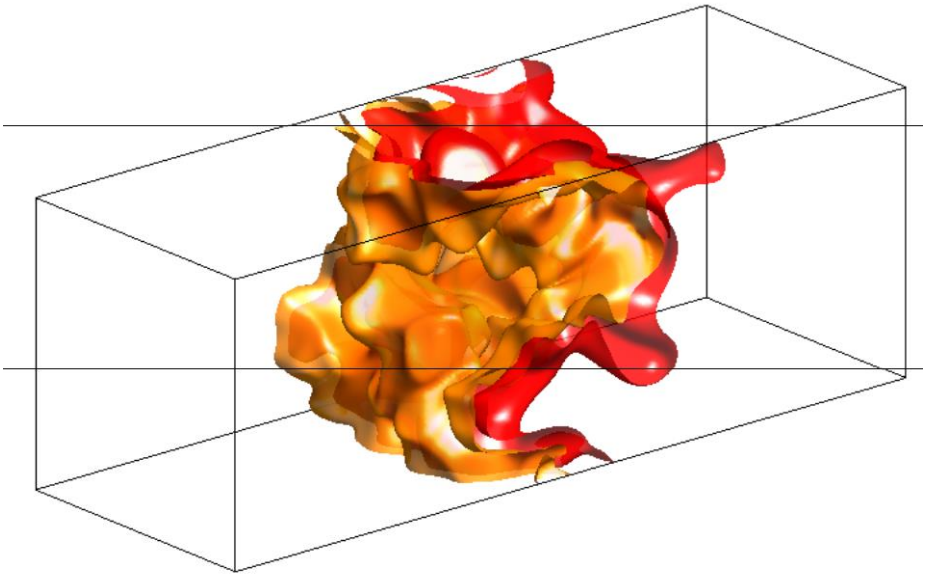

Figure 12: Planar flame with filtered forcing applied to the unburned gas side only. Results are exemplarily shown for a (high pass filter) filter size of $L_f/\delta_{th} = 5$ ($L_f/L = 0.25$) and a target velocity fluctuation of $u'/S_L = 3$.